CHAPTER 3

X-ray diffraction, optical, dielectric, elastic and viscous properties of a few bent-core nematogens

3.1. Introduction

Molecular structure and intermolecular interactions play an important role in deciding the mesogenic behavior of liquid crystalline compounds, thereby emphasizing the central importance of molecular geometry in liquid-crystallinity. In the past few decades several molecular structures with geometries diverging much from the conventional rod shape have been synthesized and studied extensively [1–3]. Among them, the bent-core or banana-shaped molecules have emerged as a field of considerable interest in soft matter research. The structural conformation of the banana molecules (i.e., introduction of a bend at the linking core between two flexible side chains) induces a spontaneous breaking of mirror symmetry and thereby leads to the formation of several unique smectic and columnar mesophases [4–6], which have no counterpart in the field of calamitic liquid crystals (LCs). Although the steric hindrance induced by the bent geometry strongly distorts the symmetry of banana molecules, the existence of distinct thermotropic mesophases including nematic ones with special mesomorphic behavior have also been revealed in few of them [5–7]. In recent years extensive research works have been carried out to synthesize new mesogenic compounds with low clearing temperature and broad nematic range [8]. Properties like occurrence of spontaneous and field induced biaxiality [9–12], smectic like cybotactic-

clusters [13, 14], in-plane polar order and chirality even in the absence of any asymmetric molecular fragment [4–6, 15–16], great flexoelectricity [17, 18], extraordinary electroconvection patterns [19–21] and unique rheological properties [22, 23] strongly differentiate the bent-core or banana nematics from the conventional thermotropic nematics. Another important aspect of the bent-core nematic liquid crystal which recently has become a major focal point in the liquid crystal research, is the twist-bend nematic phase [24–31]. This twist-bend structure can have potential applications in tunable diffraction grating, reflective display etc.

Besides the above functional characteristics, the discovery of polar switching in these compounds also make them potential candidates for electro-optical applications, the generation of second harmonics in non-linear optics as well as for other different high-tech applications in modern science.

From the viewpoint of the above unconventional properties, it is of great interest to investigate the basic material parameters and thereby to characterize the structure property correlations in the so called 'unconventional nematic phase' of bent-core mesogens. This chapter contains the results on the temperature dependence of birefringence, static dielectric constants, splay and bend elastic moduli, relaxation time and hence, the rotational viscosity of three members of a homologues series having terminally alkyl substituted bent-core mesogens, 4-cyanoresorcinols (**1/7**, **1/9** and **1/10**) [32]. In addition, the temperature dependence of the orientational order parameter ($<P_2>$) as obtained from X-ray diffraction measurements has also been reported. Measurements of relaxation time have been conducted by two different probing methods *viz.* capacitive decay and optical phase-decay-time measurement methods which permit a precise comparison between the two sets of values. The outcomes from these two techniques are found to be in good agreement with small deviations of about 10%–15%. The results are compared with those for the conventional straight-core nematics and explained in terms of the

appearance of short range nano-clustering and dipolar correlation in the mesophases.

3.2. Materials

The three compounds, being members of a homologous series of 4-cyanoresorcinol bisbenzoates, have been synthesized at the Institute of Organic Chemistry, Martin-Luther-University, Halle, Germany [8]. The mesomorphic behavior and the transition temperatures of these resorcinols (**1/7**, **1/9** and **1/10**) are summarized in table 3.1. All three compounds exhibit a highly correlated nematic phase (N_{cybC}) over a wide temperature range followed by a phase (CybC) comprising elongated but not yet completely fused strings of cybotactic clusters [8]. In addition, the higher homologues (**1/9** and **1/10)** also exhibit one or more non-polar, tilted smectic phases (Sm-$C_{(I)}$, Sm-$C_{(II)}$).

Table 3.1. Molecular structure and transition temperatures (°C) of the bent-core mesogens under study.

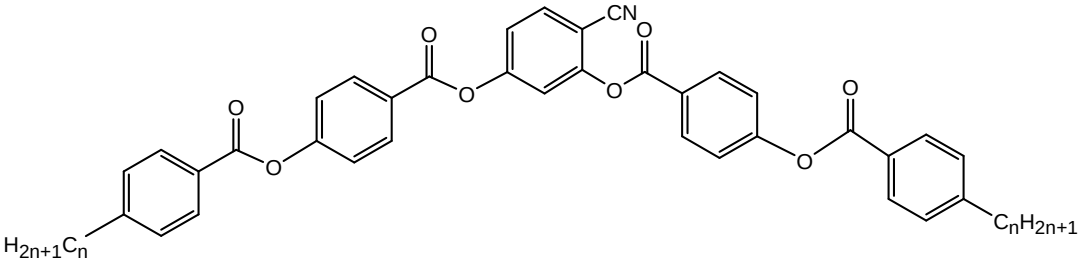

Compound	*n*	Cr		Sm-$C_{(II)}$		Sm-$C_{(I)}$		CybC		N_{cybC}		*I*
1/7	7	•	96[a]	–		–		•	40.3	•	110	•
1/9	9	•	98	–		•	52.4	•	60.5	•	105.6	•
1/10	10	•	97	•	57.1	•	68.6	•	78.6	•	104.6	•

Notes:

[a] Transition temperatures from optical transmission measurement.

•: Represents the corresponding phases are present; —: represents the absence of the phase.

The synthesis, structural investigation and phase characterization for these compounds from X-ray diffraction and electro-optical measurements have been performed by Keith *et al*. [8]. From small angle X-ray scattering measurements it has been observed that there is a clear indication of Sm-*C* like cybotactic clustering in the nematic phase which corresponds to a strong short range correlation among the bent-core molecules. Such a nematic phase may be considered as a strongly fragmented Sm-*C* phase. The dimension of those clusters again has been found to be strongly dependent on sample-temperature and length of the terminal alkyl chains in the investigated compounds [8].

3.3. Optical birefringence measurements and orientational order parameter

The temperature dependence of the birefringence ($\Delta n = n_e - n_o$) at a wavelength of λ = 632.8 nm for the three compounds is shown in figure 3.1. For all compounds on cooling, a significant increase in birefringence (Δn) has been observed within the nematic phase which is due to the increase in the nematic order and hence, enhancement in the optical anisotropy of the media. It was found that a sharp increase in Δn occurs at the I–N_{cybC} transition and then on further cooling the increase is comparatively sluggish. Such an increase in birefringence was also observed from the color change of the optical texture and was interpreted in terms of the continuous growth of the cybotactic-clusters and their uniform alignment under the condition of strong surface anchoring [8]. It may be mentioned that an attempt has also been made to measure the principle refractive indices (n_e, n_o) in the nematic phase by the surface aligned thin prism technique [33], but the transmitted intensity for both the ordinary and extraordinary rays could not be measured due to strong absorption. However, only for compound **1/7**, it was possible to measure both the refractive indices very near to the clearing temperature. The measured refractive indices obtained by this method have been plotted in the inset of figure 3.1. Agreement between the two sets of Δn values is fair in the limited temperature range.

For samples **1/9** and **1/10**, it has been found that there is an increase in birefringence, in going from nematic to Sm-*C* phase. However, throughout the entire Sm-$C_{(I)}$ or Sm-$C_{(II)}$ phases, Δn either slightly increases or remains more or less constant.

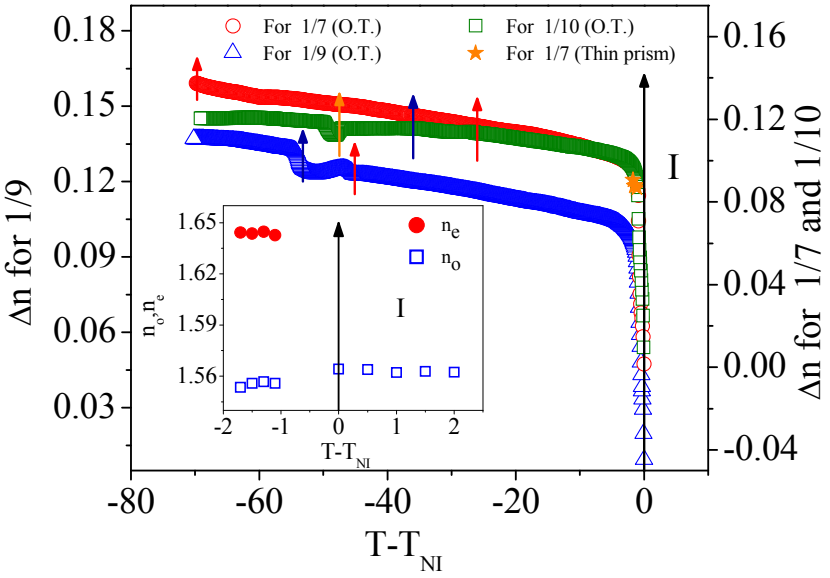

Figure 3.1. Experimental values of birefringence ($\Delta n = n_e - n_o$) as a function of temperature. (Inset) Temperature dependence of refractive indices n_o and n_e. ↑ = N_{cybC}–I, ↑ = **CybC**–N_{cybC}, ↑ = **Sm-$C_{(I)}$–CybC** and ↑ = **Sm-$C_{(II)}$–Sm-$C_{(I)}$** transitions. O.T. = Optical transmission method.

The optical birefringence Δn, obtained from the measured transmitted intensity data of the homogeneously aligned cell [34] of thickness 8.9 μm was also utilized to determine the temperature dependence of the orientational order parameter in the liquid crystalline phases of these compounds. The order parameter is defined as $\langle P_2 \rangle = \Delta n/\Delta n_0$, where Δn_0 is the birefringence in the completely ordered state and was obtained from the temperature dependence of Δn, according to the following expression [35]

$$\Delta n = \Delta n_0 \left(1 - \frac{T}{T^*}\right)^{\beta} \qquad (3.1)$$

where Δn_0, T^* and β are adjustable parameters. T^* is about 1-2 K above the clearing temperature. The exponent β depends on the molecular structure and its value is close to 0.2. It may be mentioned that this procedure is only correct for oriented phases of single axis system and for the present system the nematic phase has been considered to be macroscopically uniaxial [36]. Therefore, equation (3.1) has been fitted for all the compounds by taking the values of Δn only for the nematic phase.

The temperature dependent variation of $<P_2>$ for all the compounds is illustrated in figures 3.2(a)–(c). On cooling from the isotropic phase, similar to Δn, $<P_2>$ also exhibits a strong enhancement to a value ~ 0.6 and then remains more or less constant. The trend of temperature dependence of order parameter is found to be similar to those obtained for other banana-shaped compounds [37, 38]. However, near the I–N_{cybC} transition, the enhancement in $<P_2>$ values is comparatively much sharp owing to the strong initial growth of the clusters from the isotropic phase. Moreover, in the present case the magnitude of $<P_2>$ is found to be comparatively higher due to the presence of strong clustering. In table 3.2, Δn values at a temperature 20 K below the I–N_{cybC} phase transition for all the three compounds along with the extrapolated birefringence at the absolute zero temperature (Δn_0) and the exponent β are shown. Δn is found to be less for a compound with greater terminal chain length. A similar behavior

Table 3.2. Optical birefringence (Δn) in the N_{cybC} phase at a temperature 20 K below the I–N_{cybC} phase transition for all the three compounds under study and calculated values of Δn_0 and β (n: chain length as stated in table 3.1).

Compound (1/*n*)	**Δn**	**Δn_0**	**β**
1/7	0.1138	0.1869	0.120
1/9	0.1127	0.1813	0.118
1/10	0.1109	0.1791	0.114

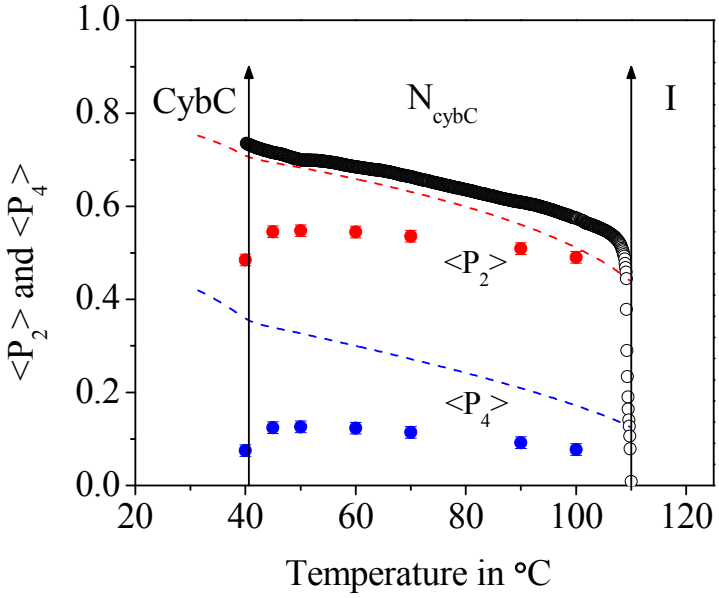

(a)

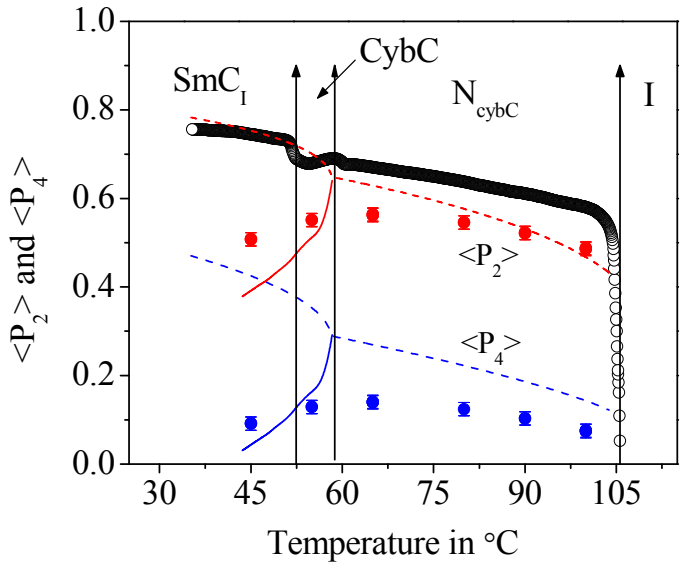

(b)

Figure 3.2. Temperature variation of $<P_2>$ and $<P_4>$ for compound (a) **1/7** and (b) **1/9**. ● **:** $<P_2>$ **,** ● **:** $<P_4>$ from X-ray diffraction method; ○ **:** $<P_2>$ from birefringence; --- : $<P_2>$, --- : $<P_4>$ from McMillan's theory; — : $<P_2>$, — : $<P_4>$ from modified McMillan's theory (after considering tilt).

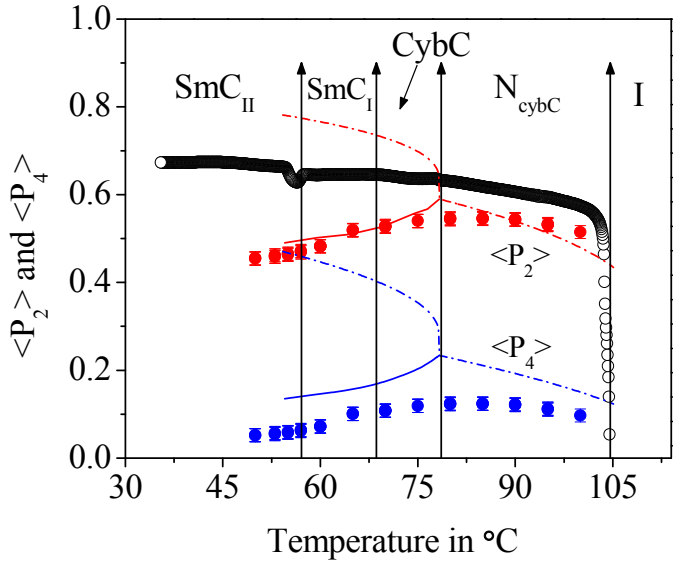

(c)

Figure 3.2. (cont'd). Temperature variation of $\langle P_2 \rangle$ and $\langle P_4 \rangle$ for compound (c) **1/10**. ● **:** $\langle P_2 \rangle$ **,** ● **:** $\langle P_4 \rangle$ from X-ray diffraction method; ○ **:** $\langle P_2 \rangle$ from birefringence; --- : $\langle P_2 \rangle$, --- : $\langle P_4 \rangle$ from McMillan's theory; — : $\langle P_2 \rangle$, — : $\langle P_4 \rangle$ from modified McMillan's theory (after considering tilt).

is also observed for the extrapolated birefringence at the absolute zero temperature, Δn_0. However, the β values are found to be relatively less than 0.2 which again may be due to the incompatibility of the Haller's procedure with the weakly first-order character of the *N–I* phase transition [39] as discussed in chapter 8.

3.4. X-ray investigations and orientational order parameter

As reported earlier [8], the X-ray diffraction patterns of oriented samples of the compounds under investigation are characterized by a diffuse scattering in the wide angle region, which indicates the fluid-like state of all the mesophases. Remarkably, in the nematic phase, the intensity of small angle scattering has been found to be much stronger than that of the wide angle scattering, suggesting the presence of smectic-like 'cybotactic' clusters [figure

3.3(a)]. For compounds **1/7** and **1/9**, the small angle scattering again demonstrates a strong temperature dependent variation in shape, intensity and position within the nematic phase. Here, with decreasing temperature, the intensity of small angle scattering has been observed to raise strongly and the related peak becomes sharper, which again indicates a continuous growth of the cybotactic clusters. However, the wide angle scattering remains nearly unaltered on varying the temperature. For the long-chain compound, i.e., compound **1/10**, a dumbbell shaped splitting has been observed for the small angle scattering analogous to the pattern obtained for skewed cybotactic nematic phases of oriented calamitic molecules. In transition from N_{cybC} to CybC phase, there was no significant change in intensity of the small angle scattering [figure 3.3(b)], but it changes to an array of distinct scatterings along with the appearance of two additional weak and relatively sharp reflections on the meridian, suggesting a phase-structure similar to that of the columnar or smectic phases [8]. The X-ray diffraction patterns in the low temperature smectic *C* phases possess significantly sharper and weak layer reflections in the small angle region [figures 3.3(c) and 3.3(d)], indicating a true layered structure.

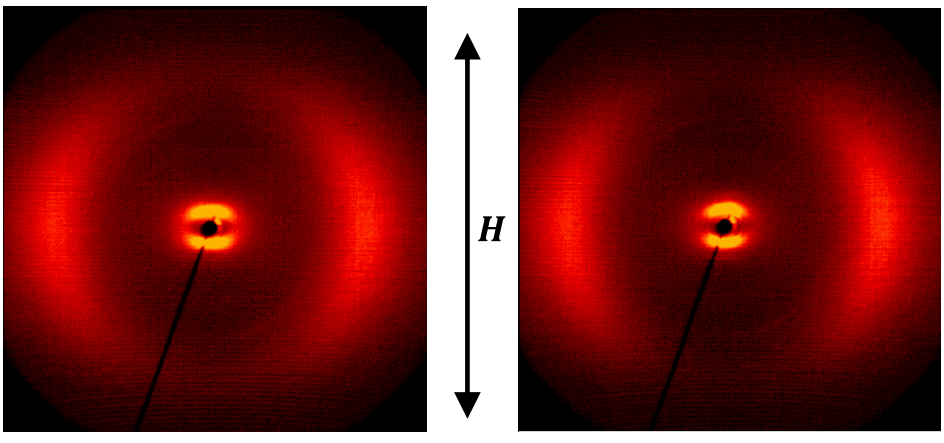

(a) (b)

Figure 3.3. X-ray diffraction patterns (wide angle) of a magnetically-aligned sample of compound **1/10**: (a) N_{cybC} phase at 100 °C, (b) CybC phase at 70 °C.

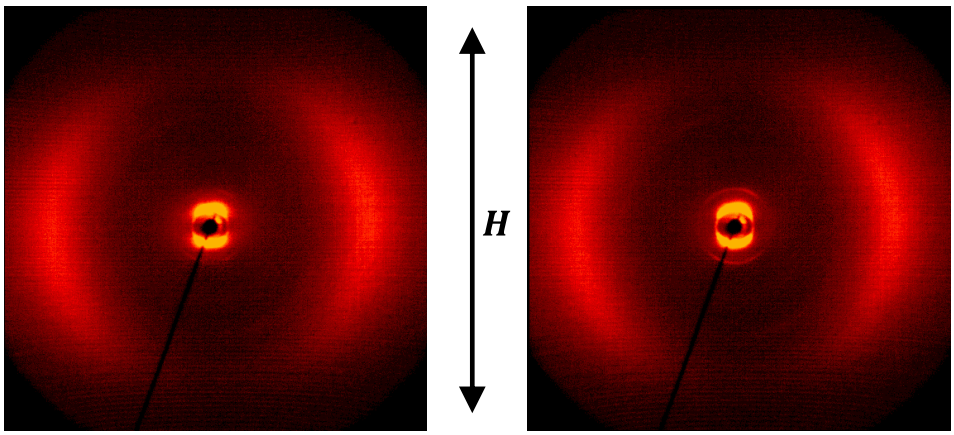

(c) (d)

Figure 3.3. (cont'd). X-ray diffraction patterns (wide angle) of a magnetically-aligned sample of compound **1/10**: (c) Sm-$C_{(I)}$ phase at 60 °C [8], (d) Sm-$C_{(II)}$ phase at 50 °C.

In this work, scattered intensity profile $I(\chi)$ (χ presents the azimuthal angle) of the outer diffused equatorial arc of the oriented samples were used to calculated the orientational distribution function $f(\beta)$ and hence, the orientational order parameter $<P_2>$ of the compounds under investigation, using the method described by Bhattacharya *et al.* [40]. The intensity data were first calibrated by those of the isotropic liquid to correct them for influences of the experimental setting using $I_{rel} = I_{phase} / I_{Iso}$, assuming an isotropic χ–distribution of the outer diffuse scattering for the sample in the isotropic phase. This calibrated intensity distribution I_{rel} were then analyzed to obtain the orientational distribution function $f(\beta)$ and the order parameter $<P_2>$ following Leadbetter's expression [41]. The temperature dependent variation of $<P_2>$ from X-ray diffraction measurements is shown in figures 3.2(a)–(c).

Although in N_{cybC} phase the trend of temperature variation of $<P_2>$ as obtained from X-ray diffraction and birefringence measurements are in agreement with one another, they show a reverse trend in the CybC and other low temperature phases. The experimental $<P_2>$ values from optical birefringence measurement increases with decrease in temperature, being accompanied with distinct changes in neighborhood of the N_{cybC}–CybC, and

CybC–Sm-$C_{(I)}$ and Sm-$C_{(I)}$–Sm-$C_{(II)}$ phase transitions, but the <P_2> values obtained from X-ray measurements drop at the N_{cybC}–CybC phase transition. In fact such drop in <P_2> with decreasing temperature also persists in the lower temperature phases, whereas <P_2> values obtained from the birefringence measurements demonstrate a completely opposite trend. This apparent contradiction between the two sets of measurements may be due to the fact that in birefringence measurement the molecules are aligned homogeneously in a thin cell where the strong surface anchoring tries to orient the molecules along the rubbing direction keeping the layers making an angle with respect to the molecular director. However, in X-ray diffraction measurements of the magnetically aligned sample, in the tilted smectic phases the molecular long axes are randomly distributed in a cone about the layer normal, hence, the observed <P_2> values determined from X-ray measurements start to decrease at the N_{cybC}–CybC phase transition and as the tilt angle increases with decrease in temperature, the <P_2> values also show a continuous decrease with decrease in temperature. The experimental orientational order parameter values from X-ray diffraction measurements have also been fitted to the McMillan's potential [42, 43]:

$$V_M(\cos\theta, z) = -v[\delta\alpha\tau\cos(2\pi z/d) + \{\eta + \alpha\sigma\cos(2\pi z/d)\}P_2(\cos\theta)] \quad (3.2)$$

where, α and δ are the two parameters of the potential, z is the displacement along the layer normal, d is the layer thickness. $\eta = \langle P_2(\cos\theta)\rangle$ is the orientational order parameter, $\tau = \langle\cos(2\pi z/d)\rangle$ is the translational order parameter and $\sigma = \langle P_2(\cos\theta)\cos(2\pi z/d)\rangle$ presents the mixed translational and orientational order parameter. Although this potential is applicable to Sm-*A* phase, but it was assumed to be valid for CybC and Sm-*C* phases as well. In this calculation, the parameter α has been varied for the different compounds, keeping the parameter δ fixed at δ = 0.16. The best fitted theoretical curves have been observed to be fairly in agreement with the experimental <P_2> values from X-ray diffraction measurements in the nematic phase, the α values

being 0.496, 0.580 and 0.662 for compounds **1/7**, **1/9** and **1/10** respectively. However, the theoretical and experimental $\langle P_2 \rangle$ values demonstrate opposite trends in the low temperature phases. As observed from the X-ray diffraction photographs [figures 3.3(c) and 3.3(d)], the molecular tilt in the low temperature tilted phases causes a broadening of the observed orientational distribution function with respect to the layer normal. This indicates that in these samples the director is randomly oriented in a cone about the layer normal. Since the layer normal is parallel to the direction of alignment and normal to the X-ray beam, the diffraction pattern is caused by the apparent orientational distribution function about the layer normal and not by the real distribution about the director. In this case, the relative orientation of the local director ($\hat{n}$), the layer normal ($\hat{k}$) and the long axis of the molecule ($\hat{l}$) is as presented in figure 3.4. Hence, one may write,

$$\cos\theta = \cos\theta_t \cos\varphi + \sin\vartheta_t \sin\varphi \cos\omega \qquad (3.3)$$

Inserting this value of $\cos\theta$ in equation (3.2), the orientational distribution function about the layer normal may be expressed as

$$f'(\cos\varphi) = N\exp - V_M(\theta_t, \varphi, \omega, z)/kT \; dzd\omega \qquad (3.4)$$

where N is a normalizing constant. Hence, from knowledge of the tilt angle (θ_t), the expression for $f'(\cos\varphi)$ can be integrated to obtain the apparent order parameter $\langle P_2(\cos\theta)\rangle_{app}$. The $\langle P_2(\cos\theta)\rangle_{app}$ values calculated using the above procedure in the CybC and Sm-*C* phases, are also depicted in figure 3.2. Here, the experimental tilt angles obtained from the X-ray diffraction measurements were only used, i.e., without introducing any adjustable parameter. Similar observations of lowering of $\langle P_2 \rangle$ values from X-ray diffraction measurements have also been reported in the tilted smectic phases of other compounds [44]. For all the compounds under investigation, the agreement between the calculated and experimental values has been found to be fairly good. Furthermore, the $\langle P_2 \rangle$ values obtained from birefringence measurement are always larger than those from X-ray diffraction by about

10%–20% in the N_{cybC} phase. Such a discrepancy is possibly due to the strong surface anchoring in thin cells of relatively smaller dimensions, leading to somewhat better alignment of the molecules within the mesophase.

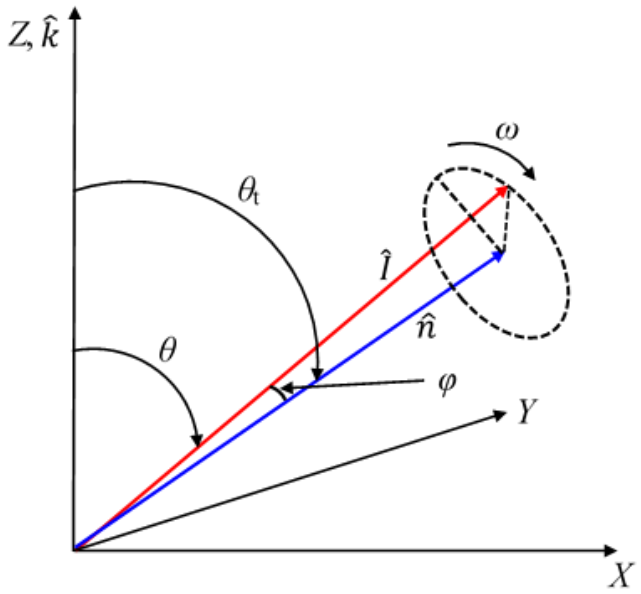

Figure 3.4. Schematic representation of molecular orientation in the Sm-*C* phases in X-ray measurements. Here, θ_t: Smectic *C* tilt angle, $\hat{n}$: molecular director, $\hat{l}$: unit vector along the molecular long axis and $\hat{k}$: unit vector along the smectic layer normal.

3.5. Static dielectric permittivity measurements

The temperature dependence of the parallel ($\varepsilon_{\parallel}$) and perpendicular ($\varepsilon_{\perp}$) components of dielectric permittivity are shown in figures 3.5(a)–(c). From the figures, it is clearly seen that compounds **1/7** and **1/9** exhibit a temperature dependant sign reversal in dielectric anisotropy ($\Delta\varepsilon = \varepsilon_{\parallel} - \varepsilon_{\perp}$) in the nematic phase. In case of compound **1/7** within the N_{cybC} phase, the anisotropy exhibits small positive values over a moderate temperature range (~ 18 °C) while for compound **1/9** the range is comparatively much narrow (~ 2 °C) and upon further cooling $\Delta\varepsilon$ becomes negative for both of them in the low temperature region. However, for compound **1/10** the anisotropy values remain negative throughout the entire mesomorphic range. These results are in agreement with

the finding of Jang *et al.* [45] and such a crossover has been interpreted as due to the presence of cybotactic clusters over the nematic phase as well as for the presence of conformers allowed by the flexible molecular core of the banana molecules. Similar sign reversal of $\Delta\varepsilon$ has also been reported by others for bent-core mesogens [46] at the *N*–Sm-C transition and also for some calamitic molecules [47]. For calamitic molecules, de Jeu *et al.* [47] accounted for such sign change at *N*–Sm-*A* transition by considering the increase in antiparallel dipolar correlation along the molecular long axis for molecules in the same layer, leading to a decrease in $\varepsilon_{\parallel}$. Sathyanarayana *et al.* [46] have concluded that apart from the argument put forward by de Jeu *et al.* [47], for bent-core mesogens the decrease in $\varepsilon_{\parallel}$ is also supported by the formation of Sm-*C* layer leading to a suppression of dielectric response along the short molecular axis while there is an effective enhancement of $\varepsilon_{\perp}$ due to the rotational hindrance of the bent-molecules emerging from the local packing of molecules in layers. Again, the decreasing temperature merely causes a significant increase in dimension of the nano-Sm-*C* clusters which thereby preferably tends to align the molecular aggregates with their planes more parallel to the cell substrate. This in effect lead to an effective increase in antiparallel correlation between the molecular dipoles along the longitudinal direction and therefore diminishes the contribution to the parallel component of dipole moment ($\mu_{\parallel}$) and hence, to $\varepsilon_{\parallel}$. An enhancement in terminal chain length also increases such short range ordering which in turn again causes decrease in $\varepsilon_{\parallel}$ values for the same reason as discussed above.

Such temperature and chain length dependant variations of cluster size have also been demonstrated by small angle X-ray diffraction measurements [8]. It is also observed that the N_{cybC}–CybC transitions are associated with a prominent change in perpendicular ($\varepsilon_{\perp}$) component of dielectric permittivity for **1/9** and **1/10** while the parallel component ($\varepsilon_{\parallel}$) remains nearly constant. For all the compounds under investigation, it has also been observed that the value of isotropic dielectric permittivity (ε_{iso}) extrapolated to the nematic phase is

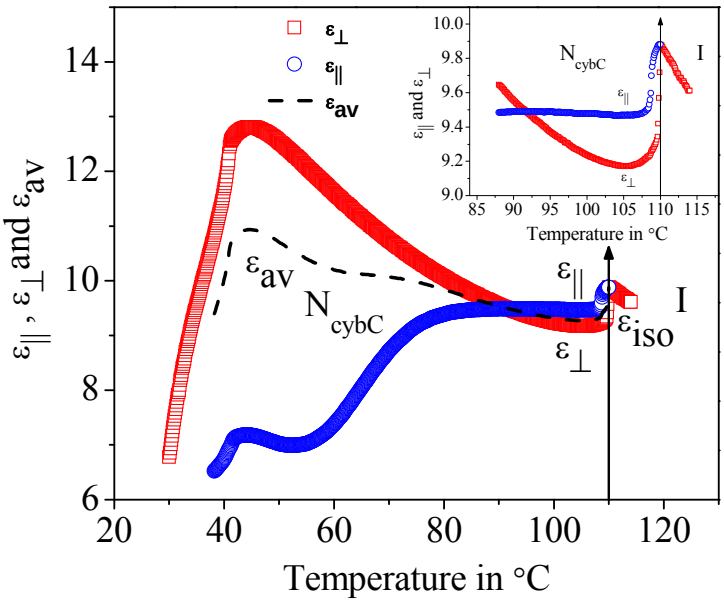

(a)

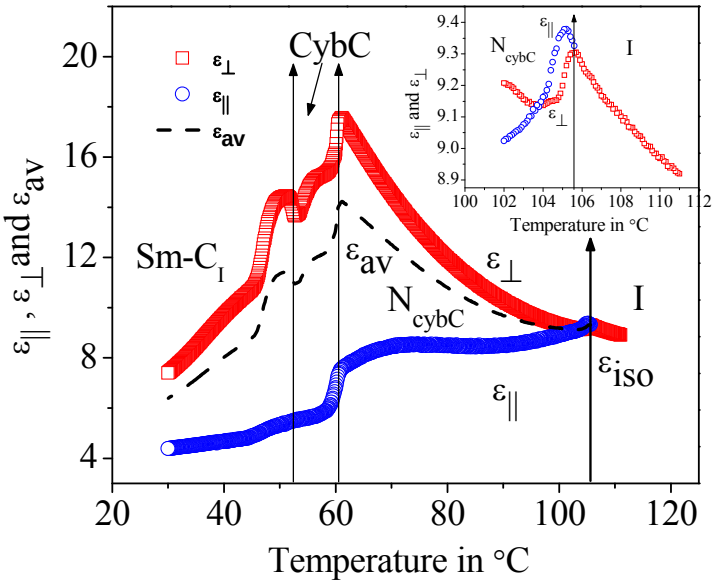

(b)

Figure 3.5. Temperature variation of dielectric parameters ($\varepsilon_{\parallel}$, $\varepsilon_{\perp}$, ε_{av}, ε_{iso}) for (a) Comp. **1/7** and (b) Comp. **1/9**.

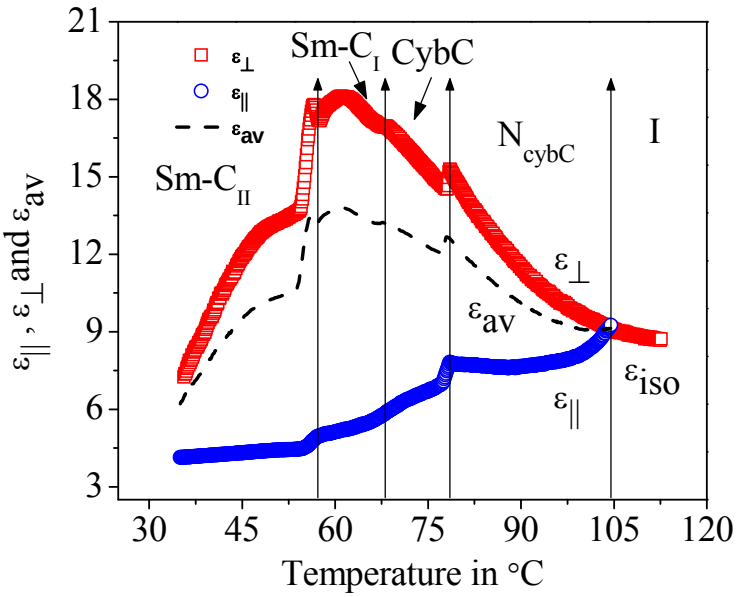

(c)

Figure 3.5. (cont'd). Temperature variation of dielectric parameters ($\varepsilon_{\parallel}$, $\varepsilon_{\perp}$, ε_{av}, ε_{iso}) for (c) Comp. **1/10**.

always greater than the average component of dielectric permittivity (ε_{av}), clearly indicating a much higher dipole-dipole interaction in the nematic phase compared to that in the isotropic phase.

3.6. Elastic constant measurements

For the present system, electrically driven Freedericksz transition could be achieved in the N_{cybC} phase by applying a field of appropriate strength. The temperature dependences of Freedericksz threshold voltage (V_{th}) for all the three compounds have been presented in figure 3.6. For compound **1/7**, in planar alignment, it has been found that the threshold voltage increases monotonically with decrease in temperature. However, in homeotropic alignment, for all the compounds it is observed that in the initial 10 °C –15 °C of the high temperature region the threshold diminishes slightly with decreasing temperature. This may be due to an initial fluctuation of alignment existing across the clusters under the condition of surface anchoring. On further

cooling, the threshold voltage remains more or less constant and then increases quite smoothly on approaching the N_{cybC}–CybC phase transition, indicating a much higher packing of molecules in the lower phase.

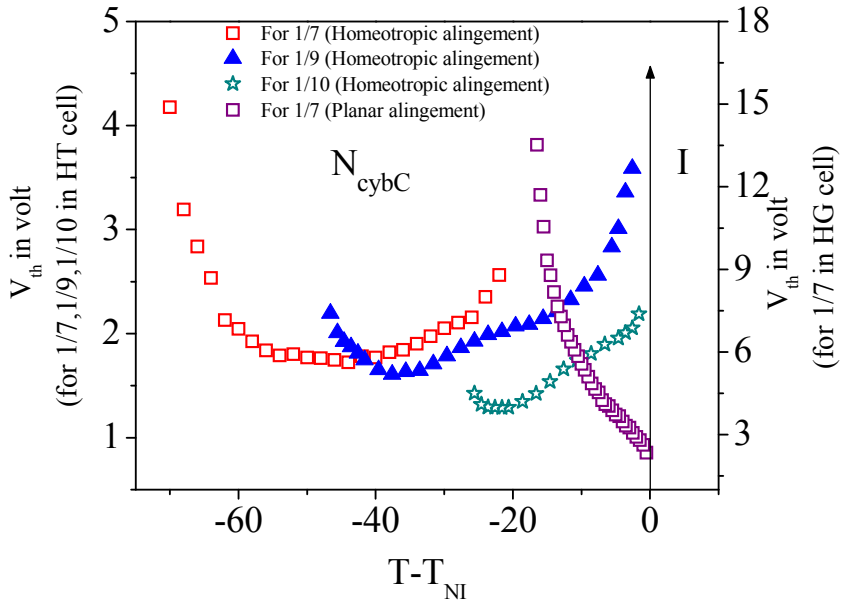

Figure 3.6. Variation of threshold voltage (V_{th}) with temperature for the resorsinol compounds.

Figures 3.7(a) and (b) show the variation of the splay (K_{11}) and bend (K_{33}) elastic constants with temperature for the three resorcinol compounds. It has been observed that the splay elastic constant (K_{11}) increases almost linearly with decrease in temperature, while the bend elastic constant (K_{33}) initially increases slowly and then diverges gradually as the CybC phase is approached. As the value of the bend elastic constant K_{33} is proportional to V_{th}^2, the divergence of K_{33} is in agreement with the divergence of threshold field. However, for compound **1/7**, the K_{11} values could not be measured in the low temperature nematic region because of the limited voltage range ($\leq$20 $V_{r.m.s}$) available in the experimental setup. From the figures 3.7(a) and (b) it is evident that although the values of K_{11} near the clearing temperature and the N_{cybC}–CybC transition are comparable to the values of K_{33}, well within the nematic range K_{11} values are always greater than corresponding K_{33} values and thereby

giving rise to negative values of elastic anisotropy (K_{33} - K_{11}). This result concurs well with the findings of Tadapatri *et al.* [48] and Sathyanarayana *et al.* [46]. For distinct bent-core mesogens they have also found negative values of elastic anisotropy and have explained this by considering coupling of bent-shaped molecules with bend-distortion in the medium [46]. Interestingly, a sign inversion of elastic anisotropy (i.e., a cross-over in the elastic moduli) was found for compound **1/10** in the high temperature nematic region. This may be due to a comparatively strong initial growth of the cluster from the isotropic state for compounds with greater terminal chain length which in turn partially hinders the coupling of individual molecule with the bend distortion thereby enhancing the K_{33} values to some extent. On a close look of figures 3.7(a) and (b), it can be verified that the same reason causes a greater slope of the temperature variation of K_{33} for compound **1/9** compared to compound **1/7** in the high temperature region.

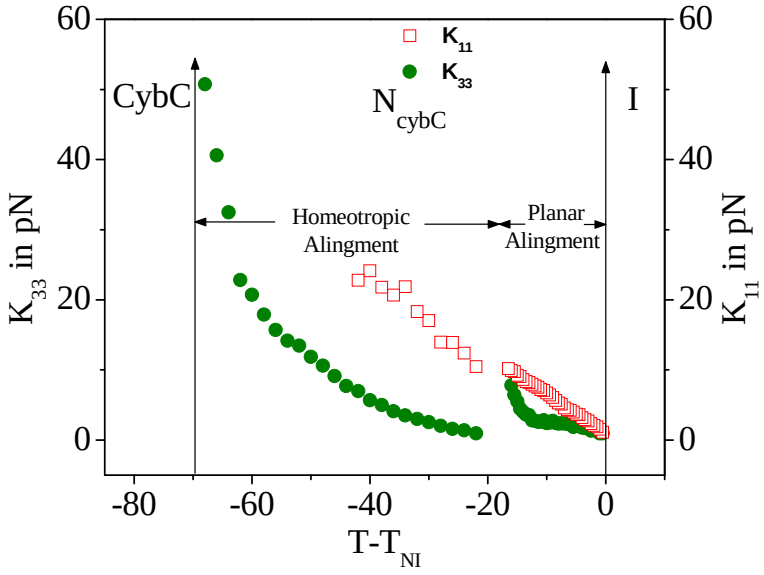

(a)

Figure 3.7. Temperature dependence of the splay (K_{11}) and bend (K_{33}) elastic constants for (a) Comp. **1/7**.

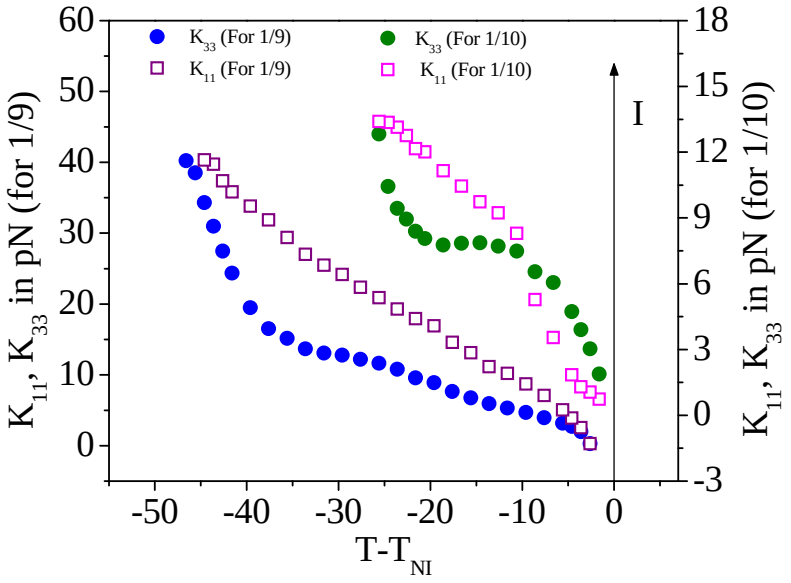

(b)

Figure 3.7. (cont'd). Temperature dependence of the splay (K_{11}) and bend (K_{33}) elastic constants for (b) Comp. **1/9** and Comp. **1/10**.

3.7. Rotational viscosity measurements

In the present study, relaxation time (τ_0) has been determined in the whole nematic range from both the optical and capacitive study of the molecular decay dynamics. Temperature variation of relaxation time (τ_0) for all the three samples have been presented in figures 3.8(a)–(b). It has been found that the results obtained from the two methods are in good agreement with a small deviation of about 10%–15%. Such small deviation between the two sets of measurements is merely due to different uncertainties involved in the two different approaches. However, the agreement is quite good near the I–N_{cybC} transition with a slight difference occurring in the low temperature region. Determination of rotational viscosity (γ_1) has also been done by utilizing equation (2.19) and the temperature variations of the same are illustrated in figures 3.9(a)–(b). Relaxation time and rotational viscosity have been found to assume a value ~ 2 s and ~ 0.5 Pa s respectively in the immediate vicinity of I–

N_{cybC} transition and then both increase monotonically with decrease in temperature. Both the values are nearly more than an order of magnitude higher compared to the conventional calamitic nematics like 4-*n*-pentyl-4'cyanobiphenyl ($\gamma_1 \sim 0.087$ Pa s at $T/T_{NI} \approx 0.965$) or 4-pentylphenyl 2-chloro-4 (4-pentylbenzoyloxy)benzoate ($\gamma_1 \sim 0.047$ Pa s at $T/T_{NI} \approx 0.965$) [49]. These results are in well agreement with the findings of Dorjgotov *et al.* [22] and Tadapatri *et al.* [48]. They have reported measurements of rotational viscosity for distinct bent-core nematics having negative dielectric anisotropy by different techniques where both have yielded γ_1 values nearly 10 times greater relative to usual straight-core mesogens. Such higher values have been explained considering the formation of temporary clusters utilizing the shape anisotropy and strong transverse dipolar contribution from the bent-core molecules [22]. The presence of such macroscopic clustering and their influence on mesophase behavior of bent-core nematics have also been demonstrated by others [13, 14, 23, 50, 51]. Small angle X-ray scattering data for these compounds clearly supports the presence of such short range Sm-*C* like ordering existing as an intrinsic phase structure throughout the entire nematic phase [8]. Moreover, on cooling the strong enhancement in γ_1 values may be attributed to the rapid growth of the clusters which in turn leads to an increase in the rotational hindrance of the molecules in aggregates. It has also been observed that on approaching the CybC phase, γ_1 values of all the compounds increases very sharply, attaining values nearly 20–30 Pa s or even more. Such a variation can merely be due to the breaking of molecular symmetry by gradual modulation of the nematic cybotactic clusters into elongated aggregates composing of stacks of Sm-*C* like ribbons, which in turn lead to the formation a 2D lattice.

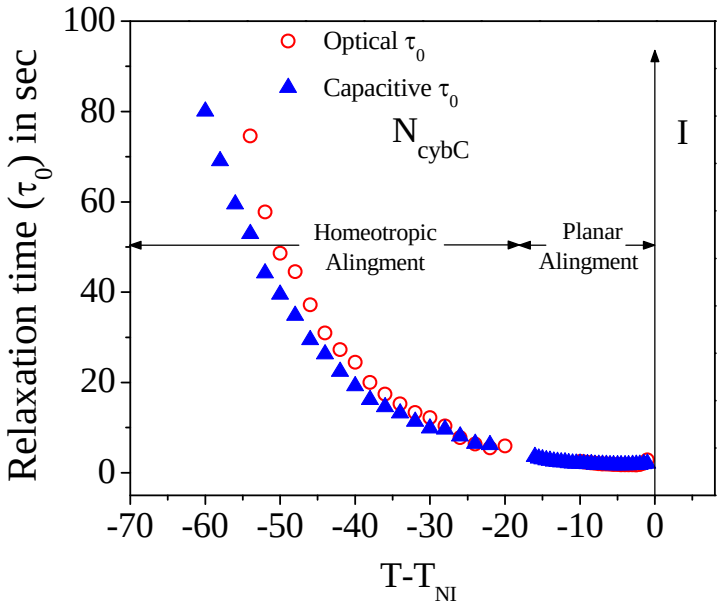

(a)

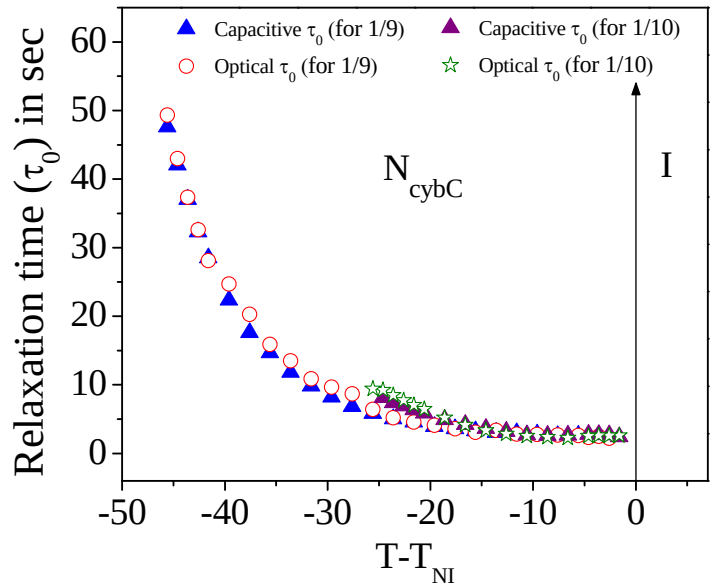

(b)

Figure 3.8. Temperature dependence of the relaxation time (τ_0) in the nematic phase for (a) Comp. **1/7**; (b) Comp. **1/9** and Comp. **1/10**, measured from both the optical method and capacitance method.

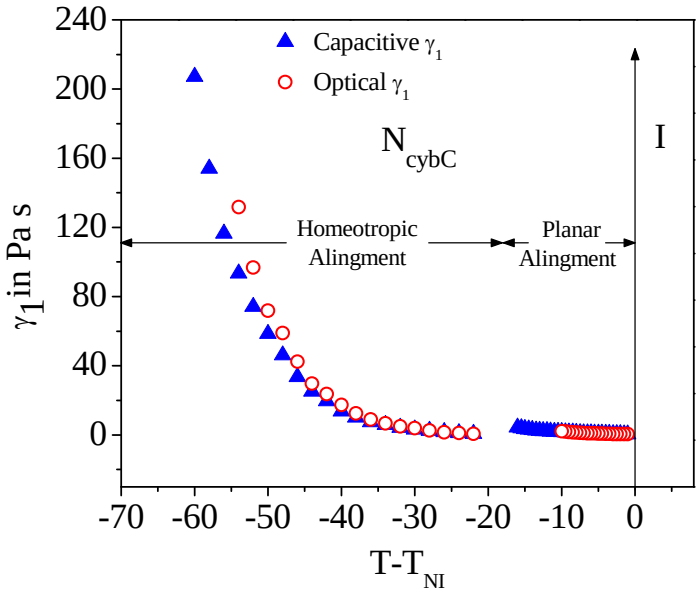

(a)

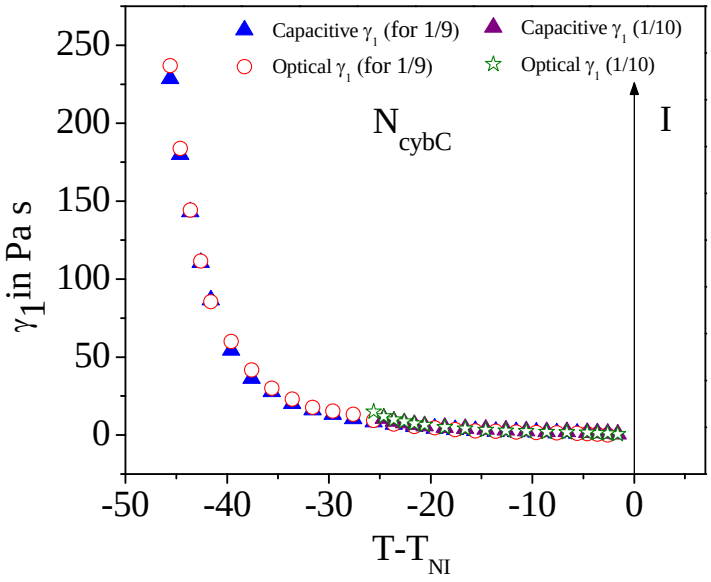

(b)

Figure 3.9. Temperature dependence of the rotational viscosity (γ_1) in the nematic phase for (a) Comp. **1/7**; (b) Comp. **1/9** and Comp. **1/10** as obtained from both the optical and capacitance methods.

For all the three compounds, evaluation of the activation energy E_a has been carried out by fitting the temperature dependence of γ_1 with the following expression using the orientational order parameter (S) from birefringence measurements:

$$\gamma_1 = \gamma_0 S \, exp\left(\frac{E_a}{k_\beta T}\right) \tag{3.5}$$

where k_β is the Boltzmann's constant and T is the temperature on the absolute scale. The variations of $\ln(\gamma_1/S)$ with $1/T$ for compound **1/9** in homeotropic alignment from both optical and capacitance methods are illustrated in figure 3.10. The slope of the Arrhenius plot can be utilized to evaluate the activation energy E_a. The activation energy (E_a) values in the nematic phase for the three compounds are listed in table 3.3. It is seen that the measured E_a values are about an order of magnitude higher than normal calamitic molecules. The probable reason may be due to the fact that in the vicinity of phase transitions,

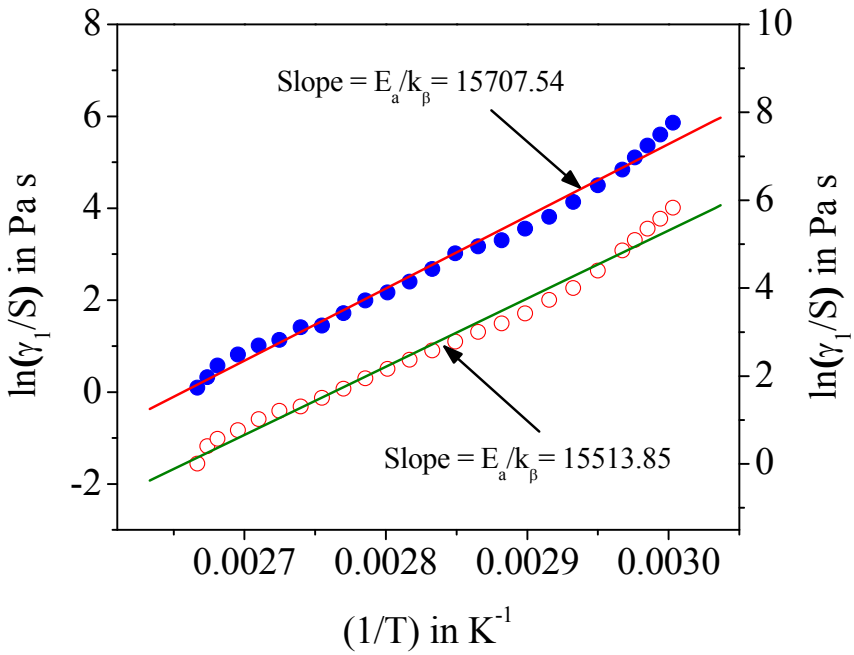

Figure 3.10. Variation of $\ln(\gamma_1/S)$ with $(1/T)$ for compound **1/9** in homeotropic alignment. (●) from optical method and (○) from capacitance method. Solid lines represent best fit of the data to equation (3.5).

due to rapid increase in cluster size, the molecular motion is affected by the strong pretransitional fluctuation which in turn leads to such quite high E_a values. However, as the E_a values that are determined are the average over the entire N_{cybC} phase, the presence of strong coupling among the smectic *C* like domains may also be responsible for such high activation energy values.

Table 3.3. Activation energy (E_a) for the three compounds under investigation. (*n*: chain length as stated in table 3.1).

Compound (1/*n*)	Activation energy (E_a) in kJ mole^{-1}	
	Optical method	**Capacitance method**
1/7	145.61	131.74
1/9	130.60	128. 26
1/10	104.52	92.50

Clearly molecular curvature plays a crucial role in determining the visco-elastic behavior of bent-shaped nematogens. Unlike conventional nematics, comprising only nearest neighbor correlation, the kink geometry of bent-molecules lead to a high lateral correlation which possibly helps in promoting short range structural aggregates composing of few Sm-*C* layers and those persists as an intrinsic constituent of the nematic phase-structure throughout the mesomorphic range. Again along with the molecular-bend, the relatively greater size of the aromatic core and alkyl chains (2 or 3 aromatic rings for calamitic molecules, otherwise their transition temperatures are too high to be investigated while 5 rings or more for bent-core molecules, where the bend reduces the transition temperatures) also helps in nano-segregation and thereby favors the formation of cybotactic clusters.

On the other hand, the bent molecular shape eventually causes a great steric force among the molecular dipoles leading to a surprisingly high shear or

flow viscosity [22]. Now unlike normal calamitics, the coupling between the shear flow and director fluctuation of bent mesogens merely elevate the γ_1 values. Recently, the study of Frank elastic moduli and effective orientational viscosities of distinct bent-core nematic by Majumdar *et al*. [52] also revealed the dramatic influence of molecular clustering on material parameters. They argued that along with the influence of clustering on the material dissipation behavior, the director distortion eventually requires a reconfiguration of cluster structure leading to higher orientational viscosities for compensating the entropy loss. This study seems to fit well with the above model where the enhancing cluster dimension obviously lead to a decrease in entropy which again in turn is counteracted by the rapid increase in γ_1 values.

3.8. Conclusions

X-ray diffraction, optical, dielectric and visco-elastic properties have been investigated in the mesophases of a few 4-cyanoresorcinols bent-core derivatives comprising a sufficiently broad nematic range. Remarkably, the molecular conformation and their association play a decisive role in determining the structure property correlations and the material parameters in the entire mesomorphic range of the investigated compounds. The temperature dependence of orientational order parameter ($<P_2>$) as obtained from the X-ray diffraction and birefringence measurements, although in agreement in the N_{cybC} phase, shows opposite trends in the low-temperature phases. Furthermore, the theoretical $<P_2>$ values, calculated using the McMillan's potential, were found to concur well with those from X-ray measurements after introducing necessary correction for the presence of molecular tilt. The dielectric anisotropy exhibits negative value over a broad region of the mesogenic range, wherein the two lower homologues (i.e., **1/7** and **1/9**) have been found to demonstrate a temperature-dependent crossover in the two dielectric permittivity components. In all the investigated compounds, the splay elastic modulus has been observed to be relatively smaller than the corresponding bend modulus in a broad

temperature range, thus leading to negative values of the elastic anisotropy. Interestingly, in compound **1/10**, a sign inversion of elastic anisotropy has been detected from positive to negative values in the high temperature region of N_{cybC} phase. The rotational viscosity values have been determined from both the capacitive decay and optical phase-decay-time measurement methods and are found to be in good agreement with only small deviations on approaching towards the low temperature phase. The yielded γ_1 values are much higher compared to the conventional calamitic nematogens and may be attributed to the formation of strong short range clustering of Sm-*C* type and their existence as an inherent part of the nematic phase structure. The strong temperature and chain length dependence of the cluster size has also clearly been reflected in the temperature variation of γ_1. Eventually such strange ordering and thereby the huge induced flow reluctance and rotational hindrance of the molecules lead to a non-Newtonian like behavior of the medium. However, the exact nature and structural behavior of the cluster and their rigorous influence on the mesogenic medium on a macroscopic scale are yet to be exploited more, which further may lead to a better understanding of the influence of molecular curvature on mesogeneity and perhaps help in designing future compounds with desirable material characteristics for practical applications.

References:

[1] S. Chandrasekhar, *Liquid Crystals*, Cambridge University Press, Cambridge (1992).

[2] N. A. Clark, Plenary Lecture 'PL2', Proceedings of the 20th International Liquid Crystal Conference, Ljubljana, Slovenia (2004).

[3] G. Cometti, E. Dalcanale, A. Du Vosel, and A. -M. Levelut, *J. Chem. Soc., Chem. Commun.*, 163 (1990).

[4] G. Pelzl, S. Diele, and W. Weissflog, *Adv. Mater.*, **11**, 707 (1999).

[5] H. Takezoe and Y. Takanishi, *Jpn. J. Appl. Phys.*, **45**, 597 (2006).

[6] R. A. Reddy and C. Tschierske, *J. Mater. Chem.*, **16**, 907 (2006).

[7] J. Etxebarria and M. Blanca Ros, *J. Mater. Chem.*, **18**, 2919 (2008).

[8] C. Keith, A. Lehmann, U. Baumeister, M. Prehm, and C. Tschierske, *Soft Matter*, **6**, 1704 (2010).

[9] B. R. Acharya, A. Primak, T. J. Dingemans, E. T. Samulski, and S. Kumar, *Pramana*, **61**, 231 (2003).

[10] L. A. Madsen, T. J. Dingemans, M. Nakata, and E. T. Samulski, *Phys. Rev. Lett.*, **92**, 145505 (2004).

[11] B. R. Acharya, A. Primak, and S. Kumar, *Phys. Rev. Lett.*, **92**, 145506 (2004).

[12] R. Stannarius, A. Eremin, M. –G. Tamba, G. Pelzl, and W. Weissflog, *Phys. Rev. E*, **76**, 061704 (2007).

[13] N. Vaupotic, J. Szydlowska, M. Salamonczyk, A. Kovarova, J. Svoboda, M. Osipov, D. Pociecha, and E. Gorecka, *Phys. Rev. E*, **80**, 030701 (2009).

[14] O. Francescangeli and E. T. Samulski, *Soft Matter*, **6**, 2413 (2010).

[15] D. M. Walba, D. J. Dyer, T. Sierra, P. L. Cobben, R. Shao, and N. A. Clark, *J. Am. Chem. Soc.*, **118**, 1211 (1996).

[16] D. R. Link, G. Natale, R. Shao, J. E. Maclennan, N. A. Clark, E. Korblova, and D. M. Walba, *Science*, **278**, 1924 (1997).

[17] J. Harden, B. Mbanga, N. Éber, K. Fodor-Csorba, S. Sprunt, J. T. Gleeson, and A. Jákli, *Phys. Rev. Lett.*, **97**, 157802 (2006).

[18] J. Harden, R. Teeling, J. T. Gleeson, S. Sprunt, and A. Jákli, *Phys. Rev. E*, **78**, 031702 (2008).

[19] D. Wiant, J. T. Gleeson, N. Éber, K. Fodor-Csorba, A. Jákli, and T. Tóth-Katona, *Phys. Rev. E*, **72**, 041712 (2005).

[20] S. Tanaka, S. Dhara, B. K. Sadashiva, Y. Shimbo, Y. Takanishi, F. Araoka, K. Ishikawa, and H. Takezoe, *Phys. Rev. E*, **77**, 041708 (2008).

[21] S. Tanaka, H. Takezoe, N. Éber, K. Fodor-Csorba, A. Vajda, and A. Buka, *Phys. Rev. E*, **80**, 021702 (2009).

[22] E. Dorjgotov, K. Fodor-Csorba, J. T. Gleeson, S. Sprunt, and A. Jákli, *Liq. Cryst.*, **35**, 149 (2008).

[23] C. Bailey, K. Fodor-Csorba, J. T. Gleeson, S. N. Sprunt, and A. Jákli, *Soft Matter*, **5**, 3618 (2009).

[24] V. P. Panov, M. Nagaraj, J. K. Vij, Yu. P. Panarin, A. Kohlmeier, M. G. Tamba, R. A. Lewis, and G. H. Mehl, *Phys. Rev. Lett.*, **105**, 167801 (2010).

[25] M. Cestari, S. Diez-Berart, D. A. Dunmur, A. Ferrarini, M. R. de la Fuente, D. J. B. Jackson, D. O. Lopez, G. R. Luckhurst, M. A. Perez-Jubindo, R. M. Richardson, J. Salud, B. A. Timimi, and H. Zimmermann, *Phys. Rev. E*, **84**, 031704 (2011).

[26] V. P. Panov, R. Balachandran, M. Nagaraj, J. K. Vij, M. G. Tamba, A. Kohlmeier, and G. H. Mehl, *Appl. Phys. Lett.*, **99**, 261903 (2011).

[27] P. A. Henderson and C. T. Imrie, *Liq. Cryst.*, **38**, 1407 (2011).

[28] D. Chen, J. H. Porada, J. B. Hooper, A. Klittnick, Y. Shen, M. R. Tuchband, E. Korblova, D. Bedrov, D. M. Walba, M. A. Glaser, J. E. Maclennan, and N. A. Clark, *Proc. Natl. Acad. Sci. USA*, **110**, 15931 (2013).

[29] C. Meyer, G. R. Luckhurst, and I. Dosov, *Phys. Rev. Lett.*, **111**, 067801 (2013).

[30] V. Borshch, Y. -K. Kim, J. Xiang, M. Gao, A. Jákli, V. P. Panov, J. K. Vij, C. T. Imrie, M. G. Tamba, G. H. Mehl, and O. D. Lavrentovich, *Nat. Commun.*, **4**, 2635 (2013).

[31] D. Chen, M. Nakata, R. Shao, M. R. Tuchband, M. Shuai, U. Baumeister, W. Weissflog, D. M. Walba, M. A. Glaser, J. E. Maclennan, and N. A. Clark, *Phys. Rev. E*, **89**, 022506 (2014).

[32] A. Chakraborty, M. K. Das, B. Das, A. Lehmann, and C. Tschierske, *Soft Matter*, **9**, 4273 (2013).

[33] A. Prasad and M. K. Das, *Phase Transitions*, **83**, 1072 (2010).

[34] A. Prasad and M. K. Das, *J. Phys.: Condens. Matter*, **22**, 195106 (2010).

[35] I. Haller, *Prog. Solid State Chem.*, **10**, 103 (1975).

[36] M. Nagaraj, Y. P. Panarin, U. Manna, J. K. Vij, C. Keith, and C. Tschierske, *Appl. Phys. Lett.*, **96**, 011106 (2010).

[37] W. Weissflog, S. Sokolowski, H. Dehne, B. Das, S. Grande, M. W. Schroder, A. Eremin, S. Diele, G. Pelzl, and H. Kresse, *Liq. Cryst.*, **31**, 923 (2004).

[38] R. Y. Dong, K. Fodor-Csorba, J. Xu, V. Domenici, G. Prampolini, and C. A. Veracini, *J. Phys. Chem. B*, **108**, 7694 (2004).

[39] J. Thoen and G. Menu, *Mol. Cryst. Liq. Cryst.*, **97**, 163 (1983).

[40] B. Bhattacharya, S. Paul, and R. Paul, *Mol. Phys*., **44**, 1391 (1981).

[41] A. K. Leadbetter and E. K. Norris, *Mol. Phys*., **38**, 669 (1979).

[42] W. L. McMillan, *Phys. Rev. A*, **4**, 1238 (1971).

[43] W. L. McMillan, *Phys. Rev. A*, **6**, 936 (1972).

[44] G. Sarkar, M. K. Das, R. Paul, B. Das, and W. Weissflog, *Phase Transitions*, **82**, 433 (2009).

[45] Y. Jang, V. P. Panov, C. Keith, C. Tschierske, and J. K. Vij, *Appl. Phys. Lett.*, **97**, 152903 (2010).

[46] P. Sathyanarayana, M. Mathew, Q. Li, V. S. S. Sastry, B. Kundu, K. V. Le, H. Takezoe, and S. Dhara, *Phys. Rev. E*, **81**, 010702 (2010).

[47] W. H. de Jeu, T. W. Lathouwers, and P. Bordewijk, *Phys. Rev. Lett.*, **32**, 40 (1974).

[48] P. Tadapatri, U. S. Hiremath, C. V. Yelamaggad, and K. S. Krishnamurthy, *J. Phys. Chem. B,* **114**, 1745 (2010).

[49] M. L. Dark, M. H. Moore, D. K. Shenoy, and R. Shashidhar, *Liq. Cryst.*, **33**, 67 (2006).

[50] S. Stojadinovic, A. Adorjan, S. Sprunt, H. Sawade, and A. Jákli, *Phys. Rev. E*, **66**, 060701 (2002).

[51] O. Francescangeli, V. Stanic, S. I. Torgova, A. Strigazzi, N. Scaramuzza, C. Ferrero, I. P. Dolbnya, T. M. Weiss, R. Berardi, L. Muccioli, S. Orlandi, and C. Zannoni, *Adv. Funct. Mater.*, **19**, 2592 (2009).

[52] M. Majumdar, P. Salamon, A. Jákli, J. T. Gleeson, and S. Sprunt, *Phys. Rev. E*, **83**, 031701 (2011).